The Astrophysical Journal, 686:1454–1465, 2008 October 20

FLUX PUMPING AND MAGNETIC FIELDS IN THE OUTER PENUMBRA OF A SUNSPOT

Nicholas H. Brummell,[1] Steven M. Tobias,[2] John H. Thomas,[3] and Nigel O. Weiss[4]

Received 2008 April 16; accepted 2008 June 28

ABSTRACT

The filamentary structure of a sunspot penumbra is believed to be magnetoconvective in origin. In the outer penumbra there is a difference in inclination of up to 30°–40° between the magnetic fields associated with bright and dark filaments, and the latter fields plunge downward below the surface toward the edge of the spot. We have proposed that these fields are dragged downward by magnetic pumping caused by the external granular convection. In this paper we model this process in a more elaborate idealized configuration that includes the curvature force exerted by an arched magnetic field in addition to magnetic buoyancy, and demonstrate that magnetic pumping remains an efficient mechanism for holding flux submerged. We discuss the implications of these results for the magnetic structure of the outer penumbra.

Subject headings: MHD — Sun: magnetic fields — Sun: photosphere — sunspots

1. INTRODUCTION

High-resolution measurements of the vector magnetic field in sunspots over the past decade have revealed the intricate and distinctive structure of the magnetic field in the penumbra. The configuration of the magnetic field, which we prefer to call an ''interlocking comb structure,'' involves a systematic difference in the inclination of the fields in the bright and dark penumbral filaments, with the inclination being greater in the dark filaments (Degenhardt & Wiehr 1991; Title et al. 1993; Lites et al. 1993; Solanki & Montavon 1993; Bellot Rubio et al. 2004; Langhans et al. 2005). Precise values of the inclination angles given by different observers differ, most likely due to differences in the inversion procedures (which are model dependent), but the general picture is the following. At the umbra-penumbra boundary the fields in the bright filaments are inclined (with respect to the local vertical direction) by about 30° and the fields in the dark filaments are inclined at about the same or a slightly greater angle. The inclinations of the fields in both components increase monotonically across the penumbra, but increase somewhat faster in the dark filaments. At the outer edge of the penumbra the inclination has reached about 70° in the bright filaments and 90°–120° in the dark filaments. In some cases the field in a dark filament has become horizontal by the middle of the penumbra.

Of particular interest in this configuration is the existence of many ''returning'' flux tubes, i.e., bundles of magnetic flux in the dark filaments that dive back below the visible surface near the outer edge of the penumbra. Naively, their existence is unexpected because the inherent magnetic buoyancy of any isolated, submerged magnetic flux tube in the field-free subphotosphere outside the sunspot would be expected to bring the tube quickly back up to the surface. The returning flux tubes demand an explanation, and the solution to the puzzle provides important insights into the overall structure and evolution of a sunspot.

We have proposed that the submergence of the returning flux tubes is caused by downward pumping of magnetic flux by the turbulent granular convection in the quiet photosphere surrounding the spot (Thomas et al. 2002; Weiss et al. 2004, hereafter Paper I). We have demonstrated the effectiveness of this flux pumping in a series of idealized numerical experiments involving three-dimensional, fully compressible magnetoconvection in a rectangular box consisting of two layers: an upper superadiabatic layer with vigorous convection, representing the solar granulation layer; and a lower layer, taken to be variously weakly stable, neutrally stable, or weakly unstable, representing the more quiescent interior region of the solar convection zone. These experiments have examined the fate of a thin layer of uniform horizontal magnetic field introduced suddenly in the upper layer of the box, in which the nonmagnetic convection has already reached a fully developed, statistically steady state. The results have all shown the flux pumping mechanism to be effective and robust.

We believe that the process of magnetic flux pumping can best be studied, at the moment, through a series of idealized numerical experiments of increasing realism (and hence increasing complexity) that contain the essential physics of the problem but are not aimed at reproducing the observations. Our numerical experiments so far have indicated that flux pumping in the granulation layer is vigorous enough to push initially horizontal magnetic fields down to the base of the granulation layer in spite of magnetic buoyancy. In a sunspot, however, the magnetic field configuration is such that magnetic curvature forces can also oppose the submergence of the field; depression of the penumbral flux tubes outside the spot increases the downward curvature of the tubes, producing an upward force. Our purpose in this paper is to present the results of new model calculations that include the effects of such magnetic curvature forces. In § 2 we present a new version of our two-layer convective model in which the initial magnetic field is in the form of a two-dimensional periodic arcade of magnetic arches, which may be thought to represent the field in a row of bipolar sunspot pairs. (Similar field structures have also been considered by Thompson [2006] and by Heinemann et al. [2007].) In our new configuration, downward flux pumping will be opposed by both buoyancy and curvature forces in much the same way as in a real sunspot. The results of our numerical experiments with this model are presented and interpreted in § 3. In § 4 we explain how these idealized results relate to the

[1] Department of Applied Mathematics and Statistics, University of California, Santa Cruz, CA 95064; brummell@soe.ucsc.edu.

[2] Department of Applied Mathematics, The University of Leeds, Leeds LS2 9JT, UK; smt@maths.leeds.ac.uk.

[3] Department of Mechanical Engineering and Department of Physics and Astronomy, University of Rochester, Rochester, NY 14627-0171; thomas@me.rochester.edu.

[4] Department of Applied Mathematics and Theoretical Physics, University of Cambridge, Cambridge CB3 0WA, UK; n.o.weiss@damtp.cam.ac.uk.

behavior of magnetic fields protruding from the penumbra of a sunspot and extending into the vigorously convecting region that surrounds it. Then we go on to consider some additional aspects of sunspot structure, emphasizing the important distinctions between the inner and outer penumbra, and conclude with a critique of the cluster model of sunspot structure and the "gappy" penumbra (Spruit & Scharmer 2006).

Magnetic flux pumping is an essential ingredient in an overall scenario that we have proposed for the formation and maintenance of a sunspot penumbra (Thomas et al. 2002; Thomas & Weiss 2004, 2008; Paper I). In brief, the sequence of events is the following. The development of an active region begins with the emergence of a large, fragmented flux tube into the photosphere. The magnetic field at the surface initially consists of numerous small magnetic flux elements that accumulate at the boundaries between granules and mesogranules to form pores without penumbrae. Magnetohydrostatic equilibrium of an individual pore requires that its magnetic field fan out with height near and above the surface because of the rapid decrease in gas pressure with height in its surroundings. Thus, the magnetic field at the outer edge of the pore is inclined to the vertical (by an average amount of about 35°). As the growing pore accumulates more magnetic flux, the inclination of the field at the outer edge of the pore increases until, at some critical angle, a convective fluting instability sets in (Tildesley & Weiss 2004). This instability, which is due to the superadiabatic temperature gradient in the layers immediately below the surface, produces a corrugation of the outer surface of the flux tube with a sinusoidal azimuthal variation of the field inclination around the circumference of the pore. (The existence of this convective fluting instability is indicated by idealized model calculations; see the discussion in § 8 of Paper I.) The nonlinear development of this instability leads to a configuration in which the spokes of more inclined field are depressed sufficiently to subject them to magnetic flux pumping by the surrounding granulation, which depresses them yet further below the surface outside the spot, thus producing the returning flux tubes.

2. THE MODEL PROBLEM

We represent key aspects of magnetic pumping around a sunspot by an idealized local model in Cartesian geometry. The equations governing three-dimensional, fully compressible, nonlinear magnetoconvection in an ideal gas (with $\gamma = 5/3$) are solved numerically in a rectangular box $\{0 \le x \le x_m, 0 \le y \le y_m, 0 \le z \le z_m\}$, where x, y, z are Cartesian coordinates with the z-axis pointing downward. The evolution of the density (ρ), velocity ($\boldsymbol{u}$), temperature (T), and magnetic field ($\boldsymbol{B}$) is governed by the continuity, momentum, energy, and induction equations, respectively. The nondimensional versions of these equations are given in Paper I. In order to ensure that the magnetic field is solenoidal, we introduce poloidal and toroidal potentials, $\mathcal{P}$ and $\mathcal{T}$, such that

$$\boldsymbol{B} = \nabla \times \nabla \times [\mathcal{P}(x,y,z)\hat{\boldsymbol{z}}] + \nabla \times [\mathcal{T}(x,y,z)\hat{\boldsymbol{z}}] \quad (1)$$

$$= \left(\frac{\partial^2 \mathcal{P}}{\partial x \partial z}, \frac{\partial^2 \mathcal{P}}{\partial y \partial z}, -\nabla_h^2 \mathcal{P}\right) + \left(\frac{\partial \mathcal{T}}{\partial y}, -\frac{\partial \mathcal{T}}{\partial x}, 0\right), \quad (2)$$

where $\hat{\boldsymbol{z}}$ is a unit vector pointing downward and $\nabla_h^2 = \partial^2/\partial x^2 + \partial^2/\partial y^2$.

Once again, we describe the depth dependence of convection by a two-layer model. The static basic state consists of a piecewise polytropic atmosphere with a polytropic index m_1 in the upper layer ($0 \le z < 1$) and a polytropic index m_2 ($m_2 > m_1$) in the lower layer ($1 < z \le z_m$). To achieve a constant heat flux, the thermal conductivity varies continuously with depth, and there is a thin transition region between the two layers. The top layer is superadiabatically stratified, with $m_1 = 1$, and the relative stability of the lower layer is then controlled by the stiffness parameter

$$S = (m_2 - m_{\rm ad})/(m_{\rm ad} - m_1), \quad (3)$$

where $m_{\rm ad} = 3/2$. We shall consider two cases: $S = 0.5$, where the lower layer is mildly stable, and $S = -0.01$, where it is marginally unstable. The remaining parameters, the Rayleigh number (Ra), the Chandrasekhar number (Q), and the diffusivity ratios (σ and ζ) are as defined in Paper I. Unless otherwise specified, we set $\sigma = \zeta = 0.1$, $\mathrm{Ra} = 5 \times 10^5$, and $Q = 3000$ in a domain with geometry $x_m = y_m = 6$ so that the convective layer has an aspect ratio of $6 \times 6 \times 1$. The depth of the lower layer and the computational resolution depend on S and are described with each case.

We impose periodic boundary conditions in the x- and y-directions, with impenetrable, rigid (zero-velocity) upper and lower boundaries; the thermal boundary conditions are that T is fixed at the top and $\partial T/\partial z$ is fixed at the bottom (cf. Paper I). In order to model the evolution of an arched structure, we require that the field be localized and predominantly vertical at the bottom boundary and horizontal at the top. The corresponding magnetic boundary conditions differ from those previously used and are more subtle. We shall restrict our attention to fields that have no mean vertical or horizontal components, when averaged over the entire domain. We assume that the upper boundary is perfectly conducting, with $B_z = 0$ at $z = 0$, and consider two options for the lower boundary. The more obvious choice is that the vertical field is prescribed in such a way that B_z is a given function of y only. In this way, we could prescribe the vertical magnetic structure emanating from the lower boundary. In this case, since the tangential components of the electric field vanish at these boundaries, it follows that

$$\partial B_x/\partial z = \partial B_z/\partial x - (1/\eta) u_x B_z,$$
$$\partial B_y/\partial z = \partial B_z/\partial y - (1/\eta) u_y B_z, \quad (4)$$

where $\eta = C_k \zeta$ and C_k is a dimensionless thermal diffusivity.

Unfortunately, this choice of boundary condition inevitably produces configurations where the strongest horizontal fields are concentrated at the lower boundary. This is demonstrated by the potential field shown in Figure 1, drawn for an example of the type of boundary variation we might want to use to produce arching structures. This field could be approximated by that of a periodic array of monopoles with alternating sign; it is then obvious that the strongest horizontal fields are at the bottom midway between the monopoles. We therefore adopt a simpler boundary condition in which the magnetic field is constrained to be vertical at the lower boundary for all time, i.e., $B_x = B_y = 0$ at $z = z_m$; together with the solenoidality condition this gives, in terms of potentials,

$$\mathcal{T} = \frac{\partial \mathcal{P}}{\partial z} = 0, \quad z = z_m, \quad (5)$$

while

$$\mathcal{P} = \frac{\partial^2 \mathcal{P}}{\partial z^2} = \frac{\partial \mathcal{T}}{\partial z}, \quad z = 0. \quad (6)$$

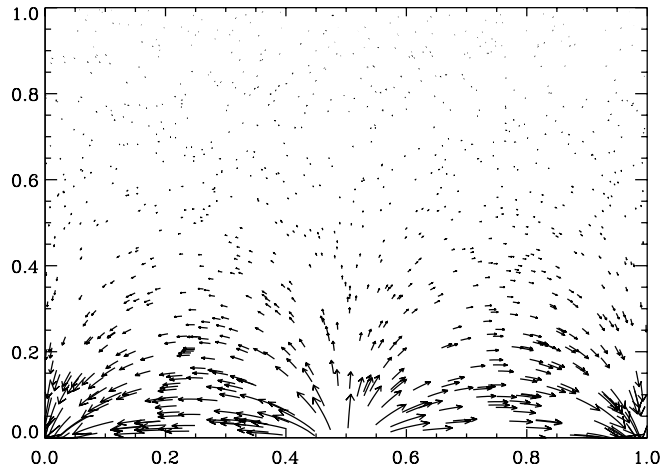

FIG. 1.—Potential field. Arrows show the magnitude and direction of a two-dimensional current-free magnetic field, with the vertical field prescribed at the lower boundary. Note that the strongest horizontal fields are at the base of the layer.

The governing equations, subject to these boundary conditions, are solved numerically using the pseudospectral scheme described by Tobias et al. (2001). The runs to be described in § 3 are initiated as purely hydrodynamic states, with no magnetic field, and are continued until a statistically steady turbulent solution is attained. At this point, a purely poloidal two-dimensional double-arched magnetic field, with $B_x = 0$, is imposed on the domain. The poloidal components of this field are derived from a flux function A via $B_y = \partial A/\partial z$ and $B_z = -\partial A/\partial y$, where

$$A(y,z) = \frac{\partial \mathcal{P}(y,z)}{\partial y} = -\frac{B_0 y_m}{4\beta}\left(\ln\left\{\cosh\left[\frac{\beta(y-y_1)}{y_m}\right]\right\} + \ln\left\{\cosh\left[\frac{\beta(y-y_2)}{y_m}\right]\right\} - \ln\left\{\cosh\left[\frac{\beta(y-y_3)}{y_m}\right]\right\} - \ln\left\{\cosh\left[\frac{\beta(y-y_4)}{y_m}\right]\right\}\right)\left\{1+\tanh\left[\frac{\lambda(z-z_0)}{z_m}\right]\right\}. \quad (7)$$

Here, we set $y_1 = 0.05y_m$, $y_2 = 0.45y_m$, $y_3 = y_m - y_2$, $y_4 = y_m - y_1$, and $\beta = \lambda = 35$, so that the field adopts the configuration shown in Figures 2*a*–2*c* and satisfies the boundary conditions above to machine accuracy. The gas density is then adjusted to maintain a magnetohydrostatic equilibrium, while keeping the temperature unchanged. The initial magnetic field is chosen to be relatively strong—but not so extreme as to force ρ to be negative. In practice, we choose the value of B_0 so that it corresponds to a Chandrasekhar number $Q = 3000$.

Our aim here is to identify the efficacy of convection in redistributing the magnetic flux from this initial arched configuration. Our choice of magnetic boundary conditions means that the magnetic field runs down and ultimately decays to zero on a resistive timescale. In order to isolate flux pumping by convection from this type of diffusive relaxation of the field, we introduce a fiducial case where no convection exists. We calculate an $S = 0.5$ case with a subcritical Rayleigh number $\mathrm{Ra} = 500$, maintaining the magnetic diffusion at the same rate as before

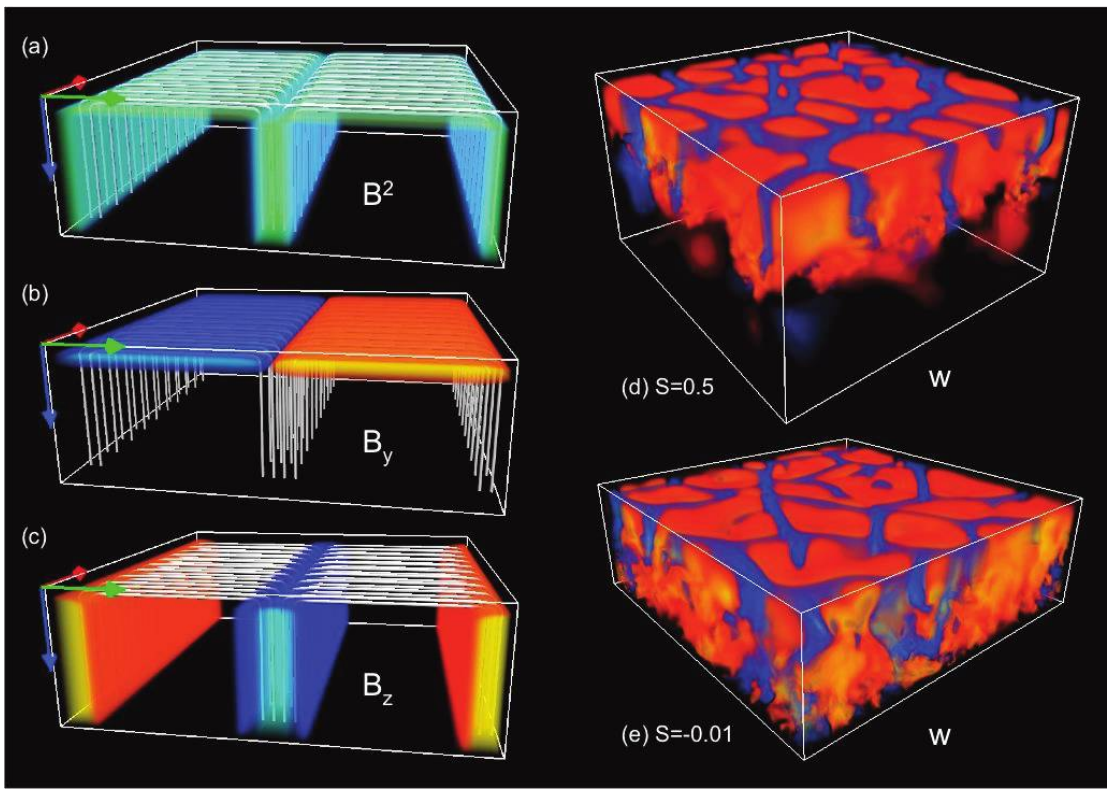

FIG. 2.—Initial conditions used. (*a*–*c*) Volume renderings of the magnetic energy density and magnetic field components comprising the initial magnetic arch conditions. Bright and opaque colors represent strong values, whereas weak values appear dark and translucent. The magnetic energy density is shown in blue-green tones, and signed magnetic fields are shown as red (positive field) and blue (negative field) tones. Also shown is a representative set of magnetic field lines (*white*). Clearly, the horizontal component is concentrated near the upper boundary. (*d*, *e*) Volume renderings of the vertical velocity, *w*, for the flows of the two cases run with varying *S*, using a red (upward) and blue (downward) color table. These color schemes will be used for all subsequent volume renderings.

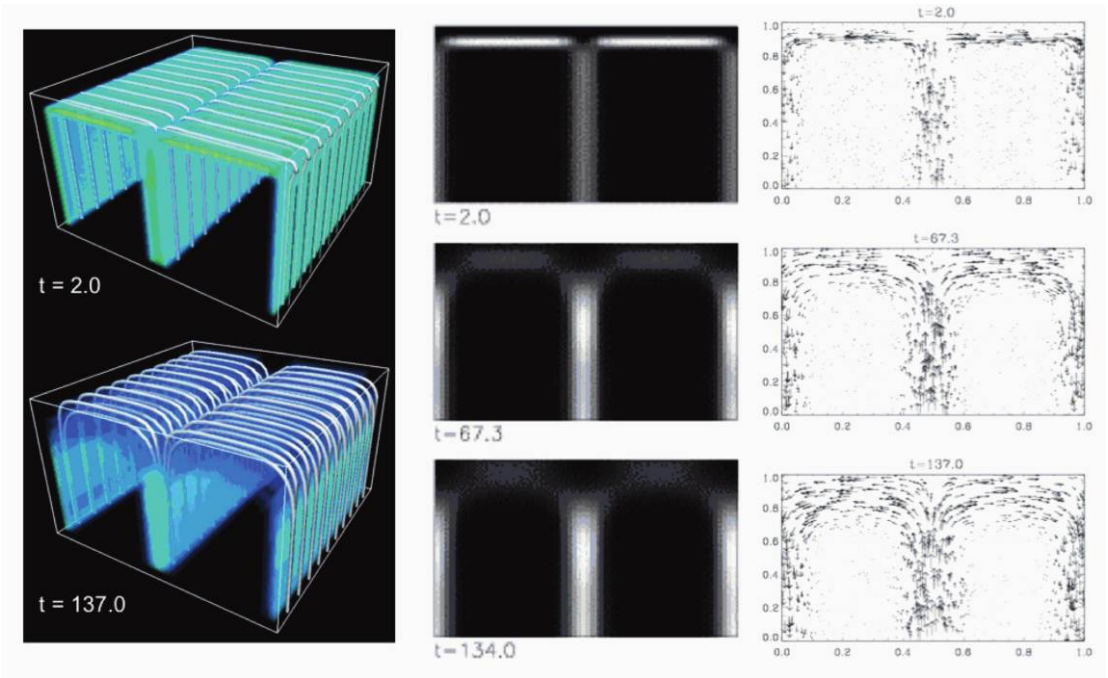

FIG. 3.—Evolution of the fiducial case. *Left*: Beginning ($t = 2.0$) and end ($t = 134.0$) of the fiducial evolution as a volume rendering of the magnetic energy density with field lines. *Middle*: Evolution of the x-averaged magnetic energy density $[\langle B^2(y,z)\rangle_x]$. *Right*: Arrows showing the magnitude and direction of the x-averaged two-dimensional magnetic field $[\langle B_y(y,z)\rangle_x, \langle B_z(y,z)\rangle_x]$. Note the very gradual change over an extremely long time.

(for constant Pr, the thermal diffusivity C_k is increased, and therefore, ζ must be reduced accordingly). This nonconvective case can be run at lower resolution ($64 \times 64 \times 98$). Figure 3 shows the time evolution of this fiducial case. Since the initial field is not force-free, it drives local motions at the start. These flows become weak and the field passes through a series of pressure-balanced configurations as the current gradually decays through ohmic diffusion. Note the degree of relaxation of the configuration in the time range ($0 < t < 134$) in this simulation.

We shall find it convenient to characterize magnetic pumping in terms of the half-box average of B_y, defined as

$$\tilde{B}_y(z) = \langle\langle B_y\rangle\rangle_{x,y}, \tag{8}$$

where in this case the y-average is taken over $0 \le y \le y_m/2$—as is clearly necessary in order to obtain a nonzero result. Figure 4 shows this half-box average at a number of different stages for the fiducial problem. Although some small redistribution of the field has occurred, most of the horizontal flux at the end of the run is still contained in the upper layer. In § 3 we contrast this behavior with two cases where turbulent convection acts so as to rearrange the field.

3. RESULTS OF THE NUMERICAL EXPERIMENTS

We now proceed to investigate the effects of magnetic pumping on this arched field configuration for two different model atmospheres. In the solar convection zone the superadiabatic gradient is large immediately below the surface, where a layer of turbulent granular convection is formed. The superadiabatic gradient falls off rapidly below this layer and convection becomes less vigorous. We first set $S = 0.5$ (cf. Thomas et al. 2002) so that the lower layer is actually stable to convection. This case is instructive as it identifies the important physical mechanisms, although the assumption of a stable lower layer is an obvious oversimplification. For this case, we set $z_m = 3.5$ with a computational resolution of $256 \times 256 \times 385$. In the second case the lower layer is weakly superadiabatic, with $S = -0.01$ (cf. Paper I). This configuration is more representative of the effects of granular and supergranular convection in the moat cell that surrounds a sunspot. Here, we use $z_m = 2.0$ with a computational resolution of $256 \times 256 \times 350$.

3.1. $S = 0.5$

In the absence of a magnetic field the overall pattern of convection is fully three-dimensional and as described in Paper I (see Fig. 2*d* and also Tobias et al. 2001). Motion is dominated by vigorous sinking plumes which penetrate downward into the stable layer below. These plumes originate at the corners of a network of cooler sinking fluid that encloses broad, gently rising, warm upflows. The sinking plumes are decelerated through buoyancy braking in the lower stable region and are brought to rest before they hit the lower boundary.

Once the magnetic field is inserted there is an immediate interaction between it and the convection. Figure 5 shows the evolution of the simulation through a number of measures. The leftmost panels of this figure show volume renderings of the magnetic energy density, where bright, light blue tones represent strong field, together with a set of magnetic field lines. It is clear from the evolution shown in the three panels that magnetic field is quickly redistributed, or "pumped," such that the strongest magnetic energy is found lower down, and field lines are moved generally lower in the domain.

The examples of magnetic pumping considered in Paper I, and also those discussed by Tobias et al. (2001), showed that the magnetic field evolves on two distinct timescales. The first phase is rapid, as magnetic flux is redistributed via the action of convection. In the second slower phase, the magnetic field relaxes through diffusion, as in Figure 3. The same distinction holds here, and we shall confine our attention to the physically relevant pumping phase only. In order to quantize the effects of pumping, we project the behavior of the three-dimensional magnetic field onto the two-dimensional y-z plane. The middle panels of Figure 5

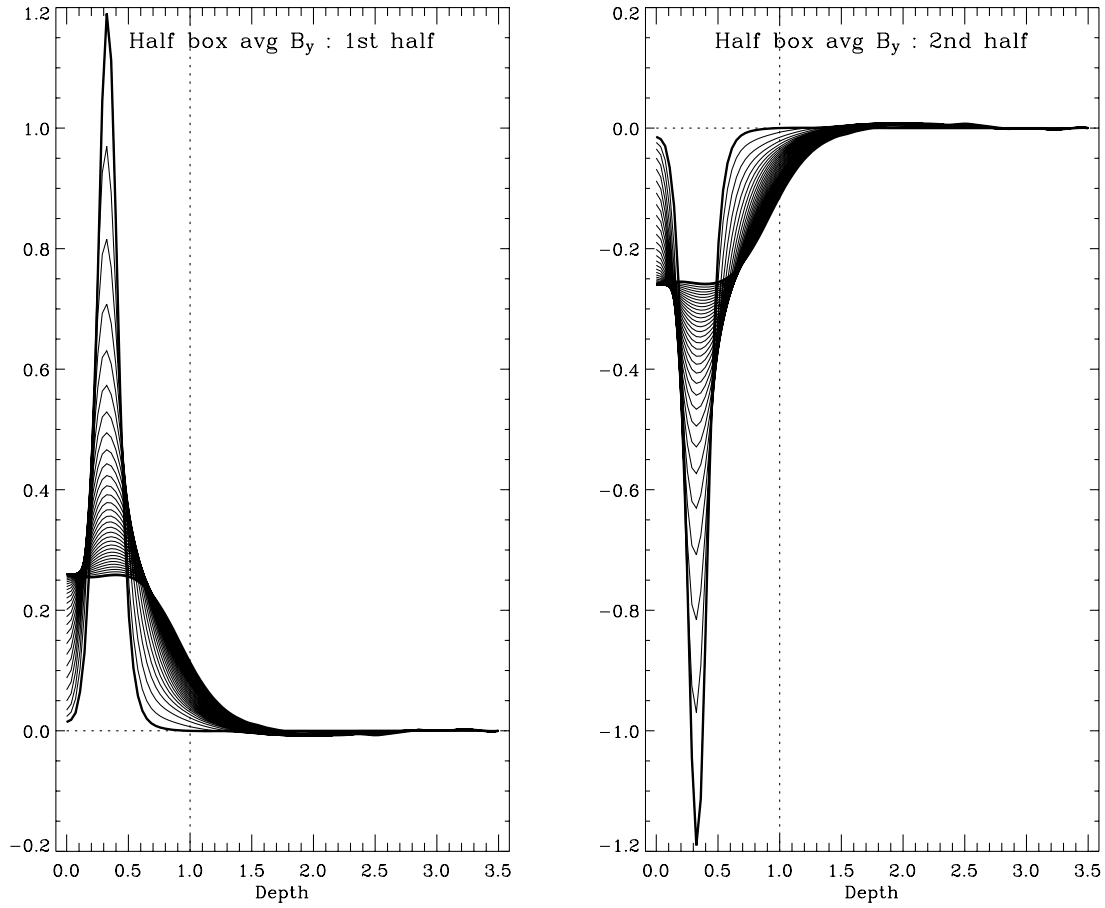

FIG. 4.—Fiducial case. Half-box averages of the horizontal field $[\tilde{B}_y(z)]$ as defined in eq. (8). Note that the field is exactly antisymmetric. Profiles are at regular intervals between times $t = 0$ and 134.0 corresponding to the panels in Fig. 3. The thick lines denote the beginning and end of the calculation. Almost all the flux remains in the upper layer.

show density plots of the x-averaged magnetic energy $\mathcal{E}_M = \langle B^2 \rangle_x$ as it evolves from its initial state. At first the field is mixed throughout the upper layer and then it is quickly pumped downward toward the interface between the two layers and eventually into the stable layer below. In this phase ($t < 4$) the rest of the field in the lower layer is scarcely altered. The evolution of the field structure is displayed in the rightmost panels of Figure 5, which show the x-averaged magnetic field, lying in the y-z plane since $\langle B_x \rangle_x = 0$. Note that the mirror symmetry of the initial field is broken owing to the effects of convection. A more quantitative measure of this process is given by following the evolution of $\tilde{B}_y(z)$ as defined in equation (8). This is shown in Figure 6. The redistribution of this flux from a strong layer centered around 0.25 toward a new peak centered just below the convective layer (at about $z = 1.5$) demonstrates what we term pumping. Note that the distribution continues to evolve slowly due to diffusion after a fast initial pumping phase.

3.2. $S = -0.01$

When the lower layer is unstably stratified, convective plumes penetrate almost to the bottom of the box, and there are associated weak upflows (see Fig. 2*e*). Motion in the upper layer does not differ significantly from the case already considered in § 3.1. Details of the purely hydrodynamic solution are displayed in Figures 5–7 of Paper I.

Figures 7–8 show the evolution of the magnetic field for this second case. As expected, the behavior in the upper layer is qualitatively similar to that found with $S = 0.5$; the magnetic field is first mixed and then pumped down toward the interface. Behavior in the lower layer is different, however, and the convective motions that are now present there have two separate effects. First, they promote the downward pumping of magnetic flux toward the base of the box, and second, they disrupt the predominantly vertical fields that were initially imposed. By $t \approx 4$ the field is pushed out of the upper layer, and by $t = 10$, the field is distributed throughout the computational domain and has lost all memory of the initial conditions, in contrast to the case with $S = 0.5$.

3.3. *Summary*

The results in this section, for both values of S, are summarized in Figure 9, which shows the evolution with time of the quantity Φ_l, defined as

$$\Phi_l = \frac{\int_{z_m}^{1} \tilde{B}_y(z)dz}{\int_{z_m}^{0} \tilde{B}_y(z)dz}. \tag{9}$$

This quantity measures the proportion of the horizontal flux that is contained in the lower layer. In this figure we display the results for all three cases that we have considered. For both cases with a vigorously convecting upper layer, a significant fraction of the flux ends up in the lower layer after the fast pumping phase is completed. When $S = 0.5$, this flux is concentrated near the interface, while it is more uniformly distributed when $S = -0.01$.

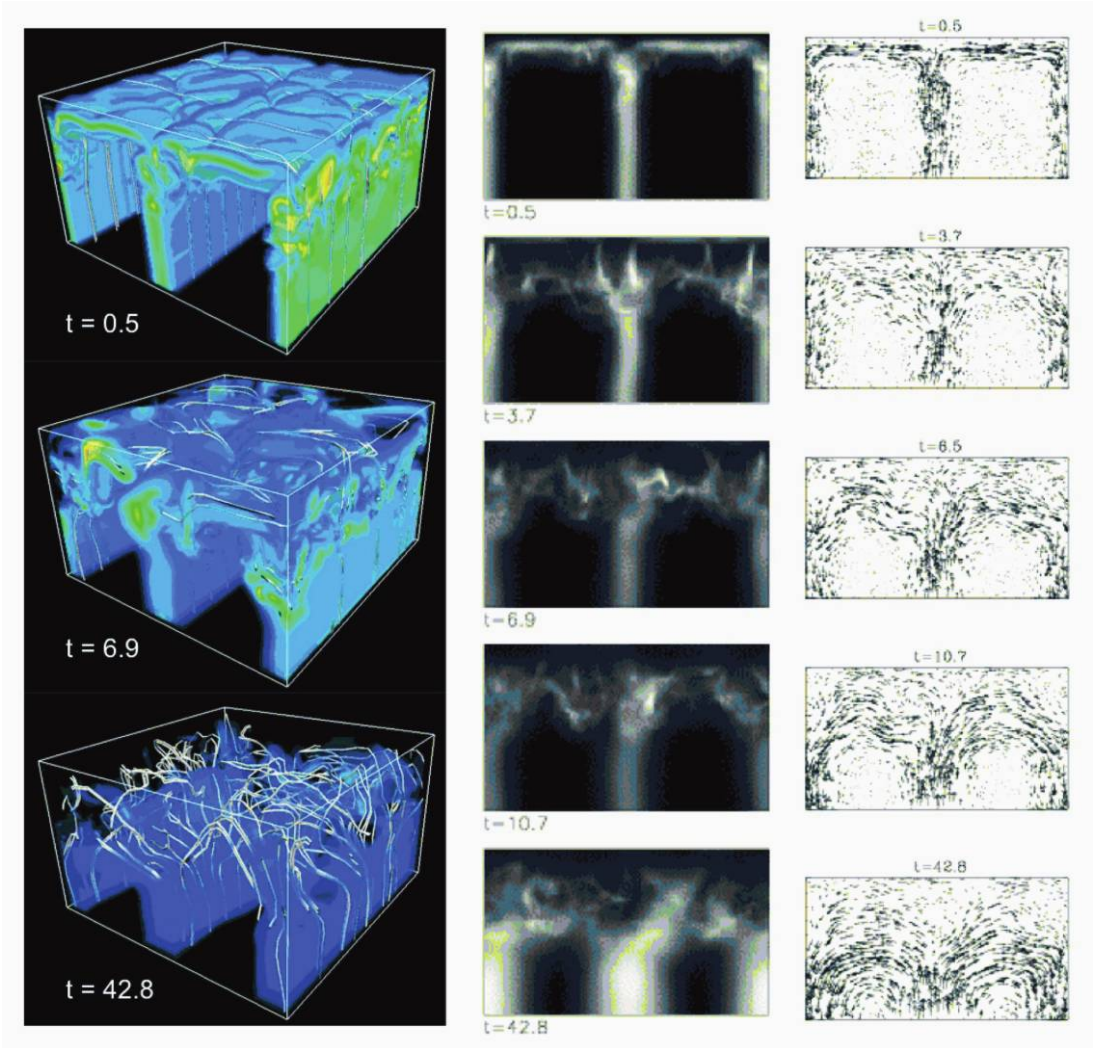

FIG. 5.— Evolution of the case with a stable lower layer, $S = 0.5$. The same series of plots is used as in Fig. 3. The average (large-scale) field is rapidly pumped out of the upper layer and concentrated at the interface with little remaining in the upper reaches of the convecting layer (*right*). The magnetic energy is also very rapidly transported away from the upper surface and toward the interface with the lower layer, but some magnetic energy associated with the small-scale magnetic field remains appreciable throughout the convecting layer (*left and middle*). Note that the evolution is completed on an interval shorter than that required to reach the second frame of Fig. 3 ($t < 43$).

By contrast, in the fiducial case, where convection is absent, flux is still trapped in the upper layer after the same amount of time has elapsed. It is only on a much longer diffusive timescale that the field eventually relaxes toward the current-free solution (Fig. 1).

4. DISCUSSION

Our new results presented above provide further support for the penumbral model described in § 1. Although the arched magnetic field configuration we employ here is still idealized, it bears a significantly greater resemblance to a sunspot than did the initially horizontal fields in Paper I. These new numerical experiments demonstrate that downward pumping of magnetic flux is indeed able to overcome the combined effects of the curvature force due to magnetic tension and the magnetic buoyancy force, and thus to submerge a significant fraction of the initial magnetic flux beneath the vigorously convecting "granulation" layer represented by the upper layer in our model. Figures 5 and 7 show many examples of bundles of strong magnetic fields that are pumped downward into the layer beneath the granulation and held there throughout the run of the calculation. Although contorted magnetic fields remain in the vigorously convecting region, the large-scale component of the field, $\tilde{B}_y(z)$, is effectively pumped downward.

4.1. *Flux Pumping and Convection outside the Penumbra of a Sunspot*

It is apparent that, while these results have no immediate application to magnetic fields in the umbra or penumbra of a sunspot, they are directly relevant to the behavior of the steeply inclined magnetic fields that protrude from the penumbra into the vigorously convecting plasma that surrounds it. Granules, with diameters of around 1000 km, are assembled into a mesogranular pattern that overlies the larger scale, more placid outflow in the annular moat cell that surrounds a spot. Thus, turbulent convection in granules corresponds to the motion in the upper layers of our models, while the radial outflow in the moat corresponds to the lower, more nearly stable layers. As in our models, the magnetic flux contained in almost horizontal fields is expelled either upward or downward. The fields expelled upward form a magnetic canopy that lies above the level of convective overshoot, at a height of about 300 km above $\tau_{500} = 1$ (Solanki 2002, 2003; Rutten et al. 2004; Puschmann et al. 2005; Cheung et al. 2007).

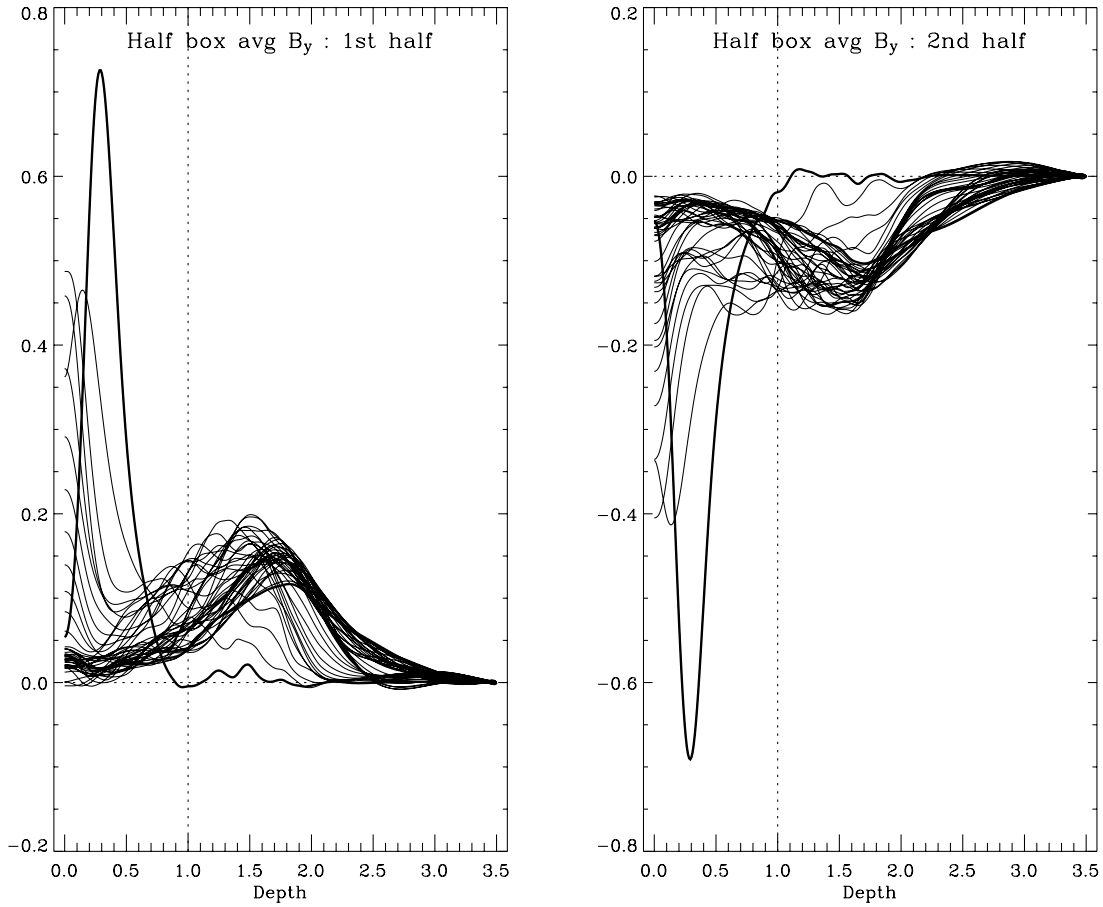

FIG. 6.—Stable lower layer, $S = 0.5$. Half-box averages of the horizontal field at times corresponding to the panels of Fig. 5. The large-scale field is pumped toward the interface. Since the convection is not constrained by symmetry considerations, the two half-boxes are no longer related by mirror symmetry as they were in Fig. 4.

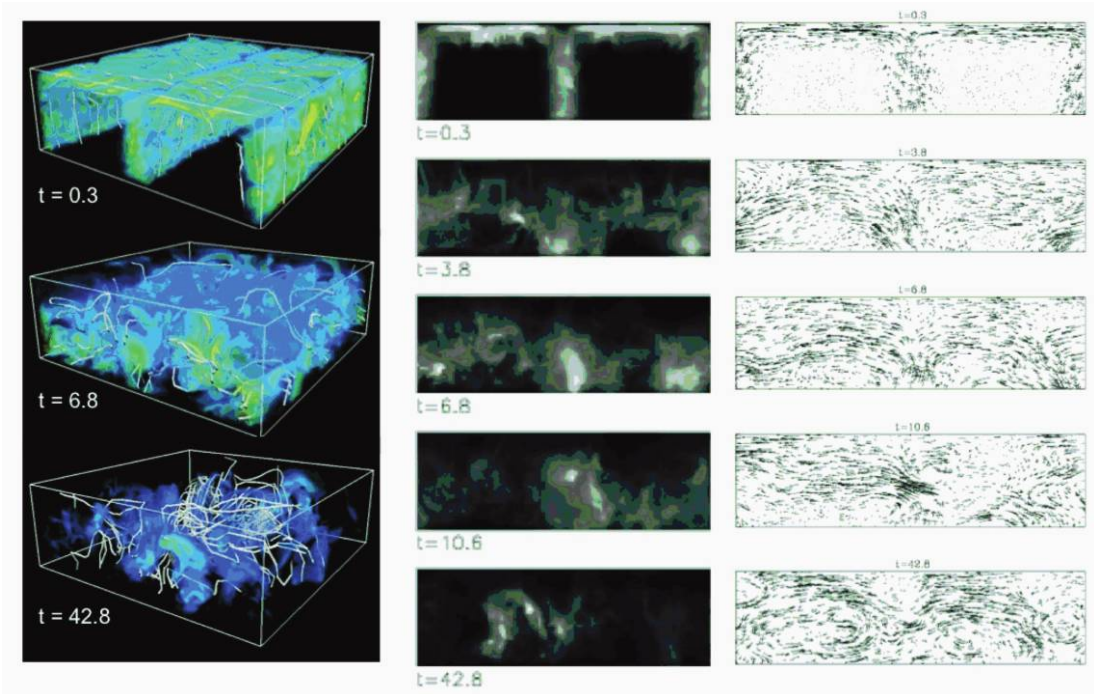

FIG. 7.—Evolution of the case with an unstable lower layer, $S = -0.1$. The same series of plots are used as in Figs. 3 and 5. The magnetic energy is rapidly transported downward and mixed throughout the whole layer. In this case, by $t \approx 10$ the vertical field is reconnected and eliminated by the weak convection in the lower layer, in contrast to Fig. 5, where the vertical field at the bottom boundary remains coherent.

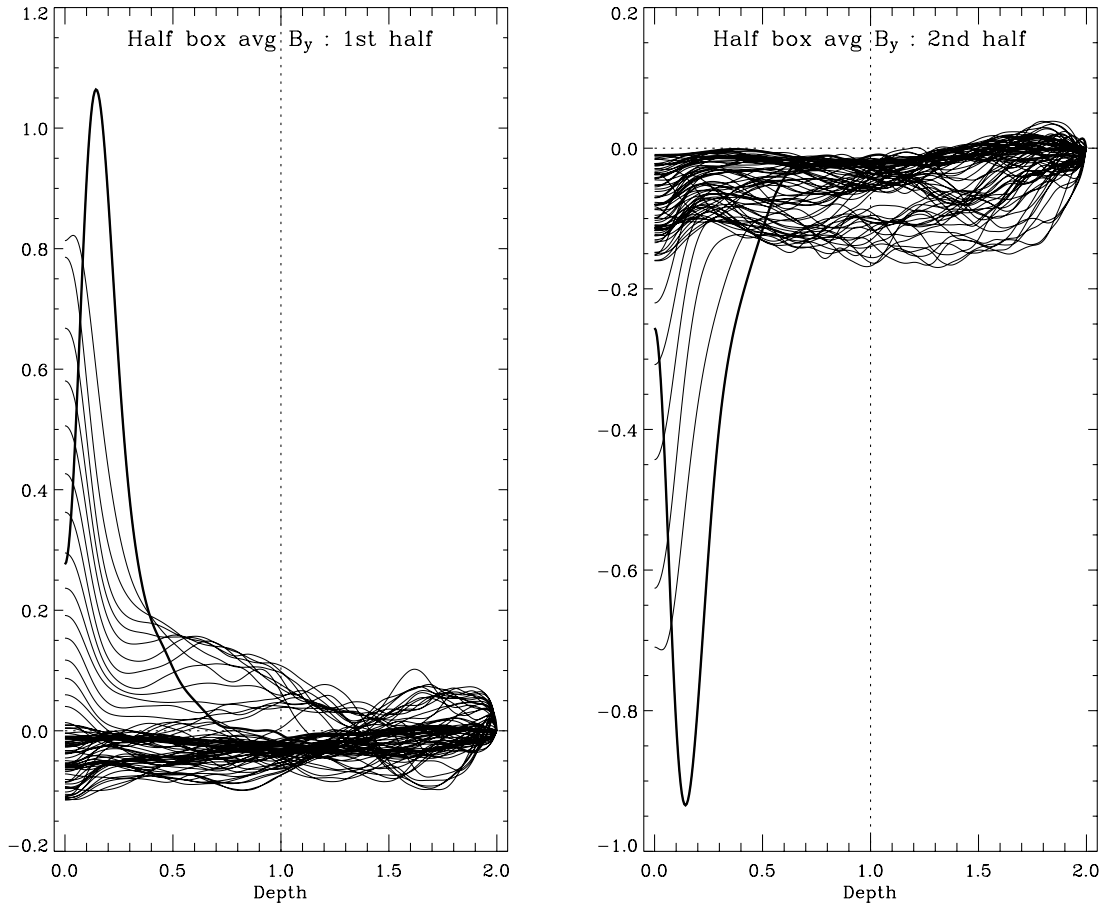

FIG. 8.—Unstable lower layer, $S = -0.1$. Half-box averages of the horizontal field at times corresponding to the panels of Fig. 7. The flux is first pumped down toward the interface and then spread throughout the layer and reduced via the interaction of convection and diffusion.

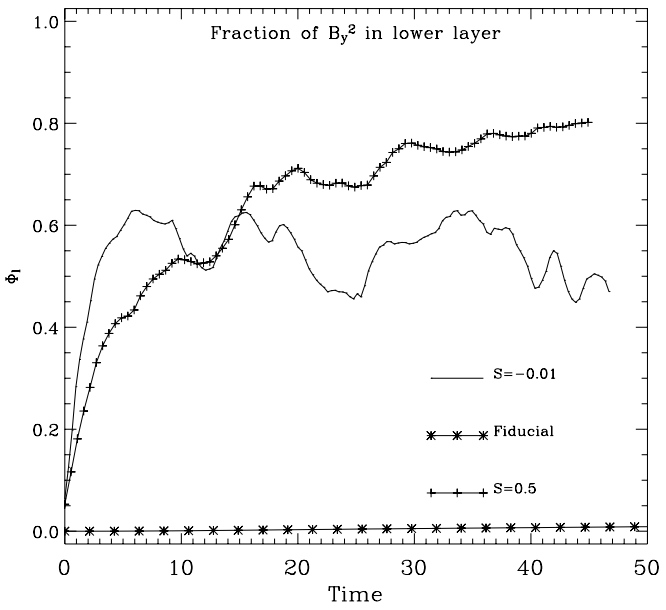

FIG. 9.—Comparison of the transport of horizontal field in the three cases. The evolution with time of the fraction of flux in the lower layer Φ_l, as defined by eq. (9), for the three cases we have considered. Clearly, both cases with convection transport the magnetic field into the lower layer much faster than would happen by nonconvective processes.

The flux expelled downward accumulates below the granules, at depths of 1000 km or more, to form an intermittent horizontal layer with radial fields that extend outward to the perimeter of the moat. Samples of these fields then appear as moving magnetic features at the photosphere (cf. Paper I).

Since the magnetic field is solenoidal, field lines are continuous and downward pumping in the moat must influence the form of the more steeply inclined fields within the penumbra. We emphasize, however, that our scenario for the origin and maintenance of the interleaved penumbral magnetic field structure does not involve flux pumping alone, but instead involves a combination of convectively driven fluting within the spot and downward pumping of the more depressed magnetic flux by turbulent convection in the external granulation. We now turn to a more qualitative discussion of this scenario and how it relates to observations.

4.2. *Inner and Outer Penumbra*

It is important to distinguish first between behavior in the inner and the outer penumbra, although the boundary between them is not uniquely determined. We find it convenient to adopt as this boundary the line separating inward- and outward-moving grains in bright filaments, at about 60% of the radial distance from the inner to the outer edge of the penumbra (Sobotka et al. 1999; Sobotka & Sütterlin 2001; Márquez et al. 2006); this line divides the penumbra into two parts with roughly equal areas. The boundary between the umbra and the inner penumbra corresponds to a transition from isolated convective plumes (in the umbra) to elongated roll-like structures in the penumbra; such a transition arises naturally as a consequence of increasing inclination of the

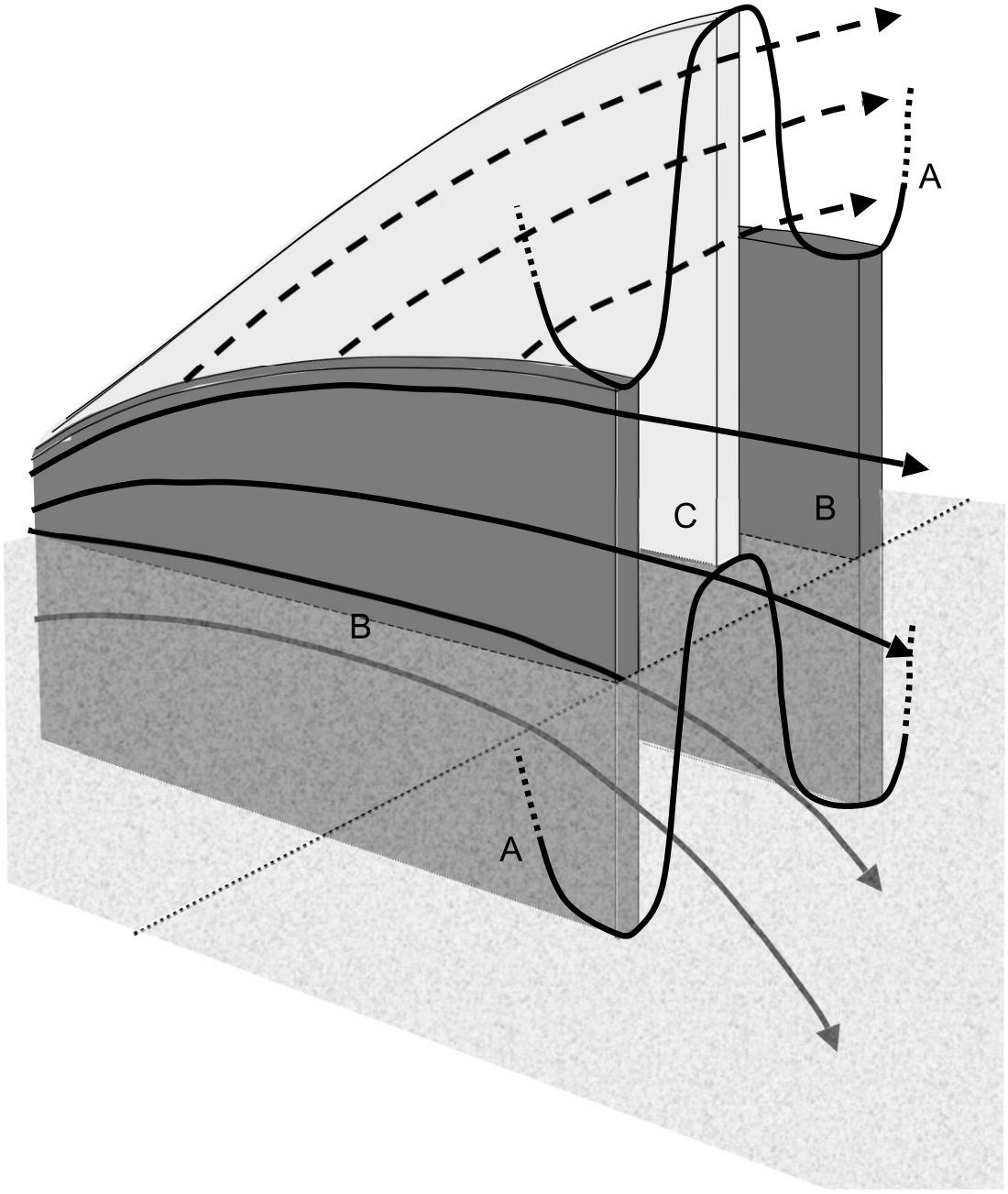

FIG. 10.— Schematic diagram of the model of the outer penumbra. Shown here is the fluted magnetopause (A) and two slabs of nearly horizontal magnetic field (*dark filaments*; B), extending downward to some depth below the solar surface and separated by a slab of less steeply inclined magnetic field (*bright filament*; C).

mean field (Thompson 2006). The outer edge of the penumbra is a ragged boundary, and prominent dark filaments protrude into the lanes between bright granules.

In the inner penumbra the bright filaments contain slender dark cores (Scharmer et al. 2002; Rouppe van der Voort et al. 2004; Langhans et al. 2007). A dark core originates at a bright feature containing an upflow (Rimmele & Marino 2006), which quickly bends over into an extended outflow along an inclined magnetic field running along the dark core (Langhans et al. 2005, 2007; Bellot Rubio et al. 2005). The fields in dark cores differ in inclination from those in the bright features that surround them (Langhans et al. 2007; Bellot Rubio et al. 2007). Estimates of this difference range from only 4°, in spectropolarimetric measurements from *Hinode* (Bellot Rubio et al. 2007), to 10°–20°, in the ground-based measurements of Langhans et al. (2007). Spruit & Scharmer (2006) have provided a convincing explanation for these dark cores, as absorption features produced by a density excess above the rising two-dimensional plume. Schüssler & Vögler (2006) point out that this corresponds to the pressure excess produced by buoyancy braking (e.g., Spruit et al. 1990) in their model of umbral convection. Furthermore, the umbral dots in their numerical model have oval shapes with dark cores and rapid flows along them; analogous fine structure has actually been detected in sunspot umbrae by observations both from the ground (Bharti et al. 2007; Rimmele 2008) and from space (Bharti et al. 2007). The same effect produces slender, elongated features in the numerical model of Heinemann et al. (2007; Scharmer et al. 2008). Near the umbra-penumbra boundary we might expect the pattern of magnetoconvection to resemble a two-dimensional version of their picture (cf. Weiss et al. 1990),

with only a modest difference in field inclination between bright and dark filaments (apart from the dark cores). Márquez et al. (2006) have exploited the technique of local correlation tracking in order to determine proper motions within the penumbra. They find apparent motions that converge on dark filaments in the inner penumbra and then move inward along them. We interpret the transverse motions as corresponding to roll-like convective flows, while the inward radial velocity is more likely to be a traveling pattern than bodily motion, as suggested by studies of traveling waves in magnetoconvection when the imposed field is inclined (Matthews et al. 1992; Hurlburt et al. 1996, 2000; Thompson 2005).

In the outer penumbra there are two distinct families of magnetic fields, with a difference in inclination of about 30° between the two interlocking field components. The magnetic fields associated with darker filaments are almost horizontal. A small fraction of the corresponding flux escapes above the surface, forming a magnetic canopy that carries an outflow and extends beyond the outer edge of the spot (Bellot Rubio et al. 2006; Rezaei et al. 2006) and is presumably related to the superpenumbra in Hα. However, the majority of the magnetic flux is actually directed downward in the outermost part of the penumbra (Langhans et al. 2005; Bellot Rubio et al. 2005).

The relationship between the outward velocity in dark cores within bright filaments and the Evershed flow in the outer penumbra remains controversial. Both Rimmele & Marino (2006) and Scharmer et al. (2008) suggest that the latter is just an extension of the former. Given the large difference in inclination between the fields in bright filaments and those in the darker filaments where the almost horizontal Evershed outflow appears, such a connection does, however, seem unlikely. We prefer to regard these features as distinct effects.

Magnetic field lines emerging from bright filaments in the outer penumbra extend upward into the corona, while those from dark filaments either hug the surface to form a canopy or plunge below the photosphere (Thomas & Weiss 2004). Thus, there can be no possibility of convective "interchanges" linking the two families. Flux pumping appears necessary in order to maintain this configuration; the penumbra has a ragged boundary, and it is significant that the most prominent dark features project outward into the lanes between adjacent rows of granules, where any magnetic fields are dragged downward by the sinking flow.

The downward extent of the horizontal fields in the outer penumbra cannot be directly observed (Borrero et al. 2006, 2008). However, the field geometry itself implies a depth not less than several hundred kilometers, for fields inclined at about 10° to the horizontal extend over 10% of the radius of the spot. Since these slabs of highly tilted field are dark, they must be deep enough for energy transport to be impeded; that suggests a depth of at least a megameter. In Paper I we put forward a rough estimate that gave a depth of around 6 Mm. Here, in the Appendix, we present a simple model that suggests that the submerged horizontal field extends over a depth of at least a quarter of the width of the penumbra and contains roughly one-sixth of the total penumbral magnetic flux.

Thus, we obtain the structure shown schematically in Figure 10, where the slab of almost horizontal magnetic field extends from just above the visible surface down to a depth of, say, 5 Mm. This differs from the "uncombed" model of Solanki & Montavon (1993), where the steeply inclined fields occupy only a thin layer that is bounded above and below near the surface. It follows from our sketch that the surface separating the sunspot from the external plasma (the magnetopause) should be corrugated. Energy radiated from the darker filaments must be supplied by transport across the field, while the brighter filaments can be supplied with energy by transport along fields that are less inclined.

4.3. *Are There Field-free Intrusions beneath the Umbra and Penumbra of a Sunspot?*

Since the magnetopause is corrugated, with fields protruding into the surrounding moat, we should also expect there to be intrusions of field-free plasma from the moat cell into the penumbra, although it is not obvious how far such intrusions may be expected to penetrate. There has in fact been a long-standing controversy between proponents of a model in which the sunspot field is composed of a tight cluster of isolated flux tubes separated by field-free regions (Parker 1979; Spruit 1981; Choudhuri 1992) and supporters of a monolithic model of the field beneath a sunspot (e.g., Cowling 1976; Jahn & Schmidt 1994), with a coherent but inhomogeneous structure (see Fig. 5 of Thomas & Weiss 1992). More recently, Spruit & Scharmer (2006; see also Thomas et al. 2006) have criticized our treatment of flux pumping and have advocated a "gappy" penumbra, with field-free regions beneath the bright filaments. It should be noted that their model is purely two-dimensional; it represents azimuthal variations of the magnetic structure in the penumbra but not radial variations.

So far as the umbra is concerned, magnetoconvection in an initially uniform vertical field offers a natural explanation of umbral dots as the bright crests of hot plumes penetrating into a stably stratified layer (e.g., Weiss et al. 1996, 2002), and this picture has now been confirmed by the realistic computations of Schüssler & Vögler (2006), which include both ionization and radiative transfer. Moreover, the cluster model might be expected to give rise to a bright network enclosing isolated dark patches (or perhaps to star-shaped bright features at junctions in such a network), contrary to the pattern of isolated umbral dots that appears in observations (e.g., Sobotka & Hanslmeier 2005) and is reproduced in the numerical simulations of Schüssler & Vögler (2006).

The field-free gaps in the penumbral model of Spruit & Scharmer (2006; see also Scharmer & Spruit 2006) are best regarded as an extreme idealization of the actual magnetoconvective situation, where the rising and expanding plumes naturally lead to local reductions of the field strength. This effect is familiar from many two- and three-dimensional model calculations (e.g., Parker 1979; Weiss et al. 1990, 2002) and is apparent also in the model of Heinemann et al. (2007). Indeed, Scharmer et al. (2008) have recently reinterpreted the gaps as being "nearly field-free."

Observations show that the magnetic field in the penumbra is more steeply inclined to the vertical above dark filaments than it is above bright filaments (e.g., Langhans et al. 2005). The more inclined component is apparently embedded in the less inclined component, for its upward extent is limited. Borrero et al. (2006) find that the more horizontal component extends no higher than $\tau_{500} \approx 3 \times 10^{-2}$, while the *Hinode* measurements of Jurčák & Bellot Rubio (2008) indicate that it only appears as τ_{500} approaches unity; the downward extent is undetermined.

In their two-dimensional model of penumbral convection, Spruit & Scharmer (2006) do not address the radial dependence of the structure. They propose that radially elongated plumes rise from field-free plasma below the bright penumbral filaments, pushing aside the ambient magnetic flux to produce stronger and more nearly vertical fields in the dark filaments. Their Figure 4 indicates that in their model the field above the bright filaments is both weaker and more steeply inclined in meridional planes. On the contrary, the observed fields above the bright filaments

are stronger and less steeply inclined (Bellot Rubio et al. 2004; Langhans et al. 2005). We do not see how their "gappy" penumbra can be compatible with these observations.

We are grateful to Thomas Rimmele and Goran Scharmer for discussing their observational results prior to publication and to the referee for helpful comments. The research described here was initiated during the program on MHD of Stellar Interiors at the Isaac Newton Institute in 2004; N. H. B., S. M. T., and N. O. W. are also grateful for the opportunity of further discussion during the Workshop on Magnetic Self-Organization in Laboratory and Astrophysical Plasmas at the Aspen Center for Physics in 2006.

APPENDIX

Here we present a simple estimate of the downward extent of the submerged horizontal magnetic field in the dark filaments at the outer edge of the penumbra. Consider a bright filament and a dark filament, each represented by a sector of a circular annulus of angular extent $\Delta\theta$. The inner radius r_1 of the annulus corresponds to the umbra-penumbra boundary, and the outer radius r_2 corresponds to the outer boundary of the penumbra. We take the magnetic field strength and inclination in the two components to be the same at radius r_1, and the field strength to drop as r^{-1} over each component. In the bright filament, we assume that the field inclination increases monotonically with radius such that the vertical component of the field is given by

$$B_z(r) = \frac{A}{r}\left[1 - \frac{r - r_1}{2(r_2 - r_1)}\right] \tag{A1}$$

for $r_1 \le r \le r_2$, where A is a constant; thus, the inclination of the field reaches 60° at $r = r_2$. We also take the magnetic field to be zero beyond the outer field lines passing through $r = r_2$, $z = 0$. The total magnetic flux emerging from the bright filament is hence

$$\mathcal{F}_b = \int_{r_1}^{r_2} \frac{A}{r}\left[1 - \frac{r - r_1}{2(r_2 - r_1)}\right] r\Delta\theta\, dr = \frac{3}{4}A\Delta\theta(r_2 - r_1). \tag{A2}$$

In the dark filament, we assume that the vertical component of the field varies as

$$B_z(r) = \frac{A}{r}\left(1 - \frac{r - r_1}{r_2 - r_1}\right) \tag{A3}$$

for $r_1 \le r \le r_2$, so that the field becomes horizontal at $r = r_2$, and we assume that the purely radial field $B_r = A/r_2$ at $r = r_2$ extends uniformly to a depth h below the surface $z = 0$. The total magnetic flux emerging from the dark filament is then

$$\mathcal{F}_d = \int_{r_1}^{r_2} \frac{A}{r}\left(1 - \frac{r - r_1}{r_2 - r_1}\right) r\Delta\theta\, dr + \int_0^h \frac{A}{r_2} r_2 \Delta\theta\, dz = A\Delta\theta\left(\frac{r_2 - r_1}{2} + h\right). \tag{A4}$$

Because this fluted magnetic field configuration can be considered to arise from an initially axisymmetric configuration, it is reasonable to assume that the magnetic fluxes $\mathcal{F}_b$ and $\mathcal{F}_d$ are equal. In this case we find that

$$h = \frac{r_2 - r_1}{4}, \tag{A5}$$

i.e., that the submerged horizontal magnetic field at the outer edge of the dark filament extends over a depth equal to one quarter of the radial width of the penumbra. Since flux pumping will further submerge this flux, we may consider this value of h to be a lower bound on the depth to which the submerged flux penetrates. Also, for this value of h the fraction of the total penumbral magnetic flux that is submerged is $A\Delta\theta h/(\mathcal{F}_b + \mathcal{F}_d) = 1/6$.

REFERENCES

Bellot Rubio, L. R., Balthasar, H., & Collados, M. 2004, A&A, 427, 319
Bellot Rubio, L. R., Langhans, K., & Schlichenmaier, R. 2005, A&A, 443, L7
Bellot Rubio, L. R., Schlichenmaier, R., & Tritschler, A. 2006, A&A, 453, 1117
Bellot Rubio, L. R., et al. 2007, ApJ, 668, L91
Bharti, L., Jain, R., & Jaaffrey, S. N. A. 2007a, ApJ, 665, L79
Bharti, L., Joshi, C., & Jaaffrey, S. N. A. 2007b, ApJ, 669, L57
Borrero, J. M., Lites, B. W., & Solanki, S. K. 2008, A&A, 481, L13
Borrero, J. M., Solanki, S. K., Lagg, A., Socas-Navarro, H., & Lites, B. 2006, A&A, 450, 383
Cheung, M. C. M., Schüssler, M., & Moreno-Insertis, F. 2007, A&A, 467, 703
Choudhuri, A. R. 1992, in Sunspots: Theory and Observations, ed. J. H. Thomas & N. O. Weiss (Dordrecht: Kluwer), 243
Cowling, T. G. 1976, Magnetohydrodynamics (Bristol: Adam Hilger)
Degenhardt, D., & Wiehr, E. 1991, A&A, 252, 821
Heinemann, T., Nordlund, Å., Scharmer, G. B., & Spruit, H. C. 2007, ApJ, 669, 1390
Hurlburt, N. E., Matthews, P. C., & Proctor, M. R. E. 1996, ApJ, 457, 933
Hurlburt, N. E., Matthews, P. C., & Rucklidge, A. M. 2000, Sol. Phys., 192, 109
Jahn, K., & Schmidt, H. U. 1994, A&A, 290, 295
Jurčák, J., & Bellot Rubio, L. R. 2008, A&A, 481, L17
Langhans, K., Scharmer, G. B., Kiselman, D., & Löfdahl, M. G. 2007, A&A, 464, 763
Langhans, K., Scharmer, G. B., Kiselman, D., Löfdahl, M. G., & Berger, T. F. 2005, A&A, 436, 1087
Lites, B. W., Elmore, D. F., Seagraves, P., & Skumanich, A. P. 1993, ApJ, 418, 928
Márquez, I., Sánchez Almeida, J., & Bonet, J. A. 2006, ApJ, 638, 553
Matthews, P. C., Hurlburt, N. E., Proctor, M. R. E., & Brownjohn, D. P. 1992, J. Fluid Mech., 240, 559
Parker, E. N. 1979, Cosmical Magnetic Fields: Their Origin and Activity (Oxford: Clarendon Press)
Puschmann, K. G., Ruiz Cobo, B., Vázquez, M., Bonet, J. A., & Hanslmeier, A. 2005, A&A, 441, 1157

Rezaei, R., Schlichenmaier, R., Beck, C., & Bellot Rubio, L. R. 2006, A&A, 454, 975
Rimmele, T. 2008, ApJ, 672, 684
Rimmele, T., & Marino, J. 2006, ApJ, 646, 593
Rouppe van der Voort, L. H. M., Löfdahl, M. G., Kiselman, D., & Scharmer, G. B. 2004, A&A, 414, 717
Rutten, R. J., de Wijn, A. G., & Sütterlin, P. 2004, A&A, 416, 333
Scharmer, G. B., Gudiksen, B. V., Kiselman, D., Löfdahl, M. G., & Rouppe van der Voort, L. M. H. 2002, Nature, 420, 151
Scharmer, G. B., Nordlund, Å., & Heinemann, T. 2008, ApJ, 677, L149
Scharmer, G. B., & Spruit, H. C. 2006, A&A, 460, 605
Schüssler, M., & Vögler, A. 2006, ApJ, 641, L73
Sobotka, M., Brandt, P. N., & Simon, G. W. 1999, A&A, 348, 621
Sobotka, M., & Hanslmeier, A. 2005, A&A, 442, 323
Sobotka, M., & Sütterlin, P. 2001, A&A, 380, 714
Solanki, S. K. 2002, Astron. Nachr., 323, 165
———. 2003, A&A Rev., 11, 153
Solanki, S. K., & Montavon, C. A. P. 1993, A&A, 275, 283
Spruit, H. C. 1981, in The Physics of Sunspots, ed. L. E. Cram & J. H. Thomas (Sunspot: Sacramento Peak Obs.), 359
Spruit, H. C., Nordlund, Å., & Title, A. M. 1990, ARA&A, 28, 263
Spruit, H. C., & Scharmer, G. B. 2006, A&A, 447, 343
Thomas, J. H., & Weiss, N. O. 1992, in Sunspots: Theory and Observations, ed. J. H. Thomas & N. O. Weiss (Dordrecht: Kluwer), 3
———. 2004, ARA&A, 42, 517
———. 2008, Sunspots and Starspots (Cambridge: Cambridge Univ. Press)
Thomas, J. H., Weiss, N. O., Tobias, S. M., & Brummell, N. H. 2002, Nature, 420, 390
———. 2006, A&A, 452, 1089
Thompson, S. D. 2005, MNRAS, 360, 1290
———. 2006, Ph.D. thesis, Univ. Cambridge
Tildesley, M. J., & Weiss, N. O. 2004, MNRAS, 350, 657
Title, A. M., Frank, Z. A., Shine, R. A., Tarbell, T. D., Topka, K. P., Scharmer, G., & Schmidt, W. 1993, ApJ, 403, 780
Tobias, S. M., Brummell, N. H., Clune, T. L., & Toomre, J. 2001, ApJ, 549, 1183
Weiss, N. O., Brownjohn, D. P., Hurlburt, N. E., & Proctor, M. R. E. 1990, MNRAS, 245, 434
Weiss, N. O., Brownjohn, D. P., Matthews, P. C., & Proctor, M. R. E. 1996, MNRAS, 283, 1153
Weiss, N. O., Proctor, M. R. E., & Brownjohn, D. P. 2002, MNRAS, 337, 293
Weiss, N. O., Thomas, J. H., Brummell, N. H., & Tobias, S. M. 2004, ApJ, 600, 1073 (Paper I)